DOI: 10.1002/cmdc.200800124

Computational Studies to Discover a New NR2B/NMDA Receptor Antagonist and Evaluation of Pharmacological Profile

Rosaria Gitto,[a] Laura De Luca,[a] Stefania Ferro,[a] Francesco Occhiuto,[b] Stefania Samperi,[b] Giovanbattista De Sarro,[c] Emilio Russo,[c] Lucia Ciranna,[d] Lara Costa,[d] and Alba Chimirri*[a]

The ionotropic glutamate NMDA/NR2B receptor and its interaction with ifenprodil-like noncompetitive ligands were investigated by a combined ligand-based and target-based approach. First, we generated 3D pharmacophore hypotheses and identified common chemical features that are shared by a training set of well-known NR2B antagonists. The binding mode of the most representative ligand was also studied by molecular docking. Because the docking results and the suggested 3D pharmacophore model were in good agreement, we obtained new information about the NR2B ifenprodil site. The best pharmacophoric hypothesis was used as a query for in silico screening; this allowed the identification of new "hit". We synthesized "hit-compound" analogues, and some of the molecules showed significant activity both in binding and functional assay as well as in vivo anticonvulsant efficacy in DBA/2 mice. The most active derivatives also exhibited neuroprotective effects against glutamate-induced toxicity in HCN-1A cells.

Introduction

N-methyl-D-aspartate (NMDA) receptors belong to the ionotropic glutamate receptor (iGluR) family and are involved in many physiological processes such as neuronal development, learning and memory, motor activity, nociception, and also in acute and chronic neuropathologies.[1–3] NMDA receptors are ligand-gated ion channels that require an obligatory co-agonist, glycine, in addition to the synaptically released neurotransmitter glutamate, for receptor activation.[4]

Functional NMDA receptors are heteromeric complexes that contain the NR1 and NR2 subunits (NR2A-D subtypes), and the NR3A subunit, which plays a regulatory role in the functioning of some NMDA receptors. The NR1 and NR2 subunits share a common membrane topology with other members of the iGluR family. Each subunit has a large extracellular amino-terminal domain (ATD), three transmembrane segments (TM1, TM3, and TM4), a pore-lining P-loop region (TM2), an extracellular loop (L3) that is located between TM3 and TM4, and an intracellular carboxy terminal domain. Further, the ATD that precedes the agonist binding domain of NMDA receptor subunits has structural similarity to the bacterial periplasmic leucine, isoleucine, valine binding protein (LIVBP).[5] By using molecular modeling and site-directed mutagenesis studies, it has been demonstrated that the LIVBP-like domain of the NR2B subunit contains the binding pocket for the NR2B antagonists.[6,7] NR2B subtype-selective antagonists are a family of compounds that have aroused research interest, and the ifenprodil prototype (**1**) served as a template to design a large number of much more selective analogues such as Ro 25-6981 (**2**), CP 101,606 (**3**), CI-1041 (**4**), Ro 04-5595 (**5**), and benzimidazole derivative **6** (Figure 1), which have been shown to selectively bind at the so-called ifenprodil site.[8–12]

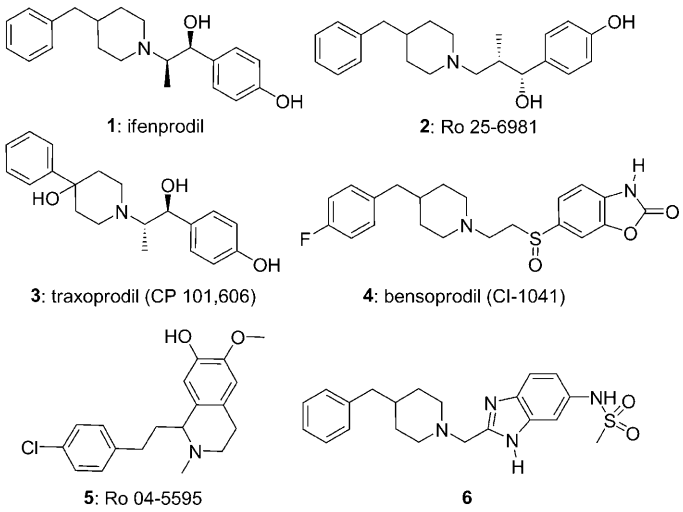

Figure 1. NR2B subtype antagonists.

These molecules showed neuroprotective effects in animal models without producing the undesirable side effects that are

[a] *Prof. R. Gitto, L. De Luca, S. Ferro, Prof. A. Chimirri*
Dipartimento Farmaco-Chimico, Facoltà di Farmacia
Università di Messina, Viale Annunziata, 98168 Messina (Italy)
Fax: (+39) 090-6402
E-mail: chimirri@pharma.unime.it

[b] *Prof. F. Occhiuto, Dr. S. Samperi*
Dipartimento Farmaco-Biologico, Università di Messina
Viale Annunziata, 98168 Messina (Italy)

[c] *Prof. G. De Sarro, E. Russo*
Dipartimento di Medicina Sperimentale e Clinica
Università Magna Græcia, Via T. Campanella, 88100 Catanzaro (Italy)

[d] *Prof. L. Ciranna, Dr. L. Costa*
Dipartimento di Scienze Fisiologiche
Università di Catania, Viale Andrea Doria 6, 95125 Catania (Italy)

associated with many nonselective NMDA receptor antagonists, and one of them, CP 101,606 (**3**, traxoprodil) is in phase II clinical trials for the treatment of strokes.[8] Recently, novel structures that contain aminoquinoline, benzamidine, and imidazole nuclei have also shown NR2B-selective NMDA antagonism and constitute new interesting pharmacological tools.[10,12–14] In the context of this study, our aim was to identify new chemical entities that are able to interact with the NR2B ifenprodil site.

We thus planned a molecular modeling strategy to develop a 3D pharmacophore model with the intent of using the obtained hypothesis as a query to screen commercially available databases. The hits that were obtained during this screening procedure were purchased and experimentally tested in a binding assay. Molecular docking studies were also performed with the most representative ligands in an attempt to explore the binding modes of noncompetitive antagonists. A selected hit represented a template to design new ligands, and the first synthesized compounds were tested to evaluate their anticonvulsant activity in DBA/2 mice; for the most active derivative, the binding and functional activity as well as neuroprotective efficacy were also studied.

Results and Discussion

Molecular modeling studies

A combined ligand-based and target-based approach was performed through the following steps: 1) generation of 3D pharmacophore hypothesis; 2) docking studies to describe the binding pocket and the main interaction of a selective ligand; 3) comparison of the results of the structure-based and ligand-based studies; 4) search on 3D database by employing the pharmacophore hypothesis; 5) identification of new chemical entities.

For pharmacophore model generation we used the HipHop algorithm that is implemented in the Catalyst software package version 4.10. HipHop compares diverse molecules to derive 3D hypotheses based on common chemical features, without considering the degree of pharmacological activity.

Six molecules (**1**–**6**, Figure 1) among the most representative NR2B antagonists were selected as the training set, and compound **2** was considered to be the most relevant compound because of its very high selectivity and affinity for NR2B subunit.[7] Catalyst provides a dictionary of chemical features that are found to be important in drug–enzyme/receptor interactions. These are hydrogen bond donors, hydrogen bond acceptors, aromatic ring, hydrophobic (aliphatic or aromatic) groups, and positive and negative ionizable groups. On the basis of the atom types in the molecules of the training set, the following chemical functions were selected for the hypothesis generation: hydrogen bond donor, hydrogen bond acceptor, hydrophobic group, hydrophobic aromatic region and positive ionizable group.

Among the ten hypotheses that were obtained, the top-ranked one with a ranking score of 93.3294 was chosen for further analysis. This pharmacophore model contained six chemical features: one positive ionizable (P), one hydrophobic aromatic (Z), two hydrophobic sites (H1, H2), one hydrogen bond donor (D) and one hydrogen bond acceptor (A).

Previously, SAR studies suggested that some chemical features were critical for binding affinity at NR2B receptor: 1) a phenolic OH group as a H-bond donor, 2) two aromatic rings, and 3) a basic nitrogen atom, which might serve for electrostatic interaction.[15] Furthermore, on the basis of site-directed mutagenesis, a possible binding mode was proposed for Ro 25-6981 (**2**) in which the protonated nitrogen atom forms an electrostatic interaction with the carboxyl group of D101 and the benzyl group establishes an aromatic stacking (π–π) interaction with the side-chain of F176.[7] Our obtained pharmacophore model confirmed these previous findings and Figure 2 shows the best-fitted conformer of Ro 25-6981 (**2**)

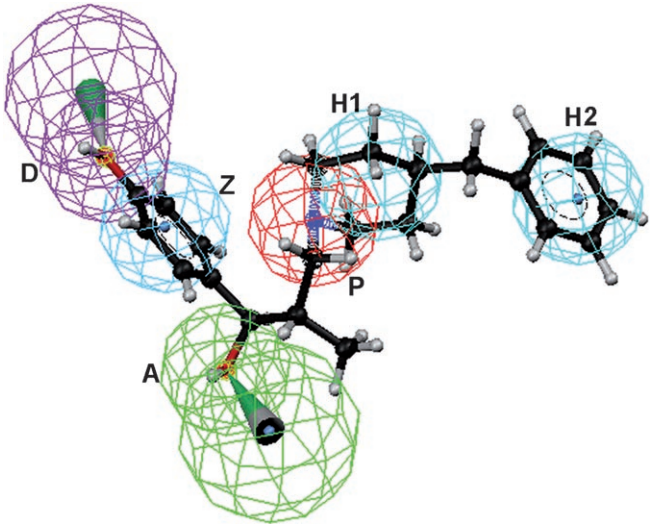

Figure 2. Mapping of Ro 25-6981 onto the Catalyst/HipHop pharmacophore model. Pharmacophoric features are: one positive ionizable (P, red), one hydrophobic aromatic (Z, light blue), two hydrophobic (H, cyan), one hydrogen bond donor (D, magenta), and one hydrogen bond acceptor (A, green).

into the 3D hypothesis: 1) hydrogen-bond donor site (D) that is mapped by the phenolic OH group; 2) one hydrophobic aromatic area (Z) that is occupied by the phenyl ring and one hydrophobic feature (H2) mapped by the benzyl ring; 3) a positive ionizable center (P) that is occupied by the nitrogen of the piperidine nucleus. Moreover, this study provided further information about additional chemical functions that are important for NR2B antagonists: 4) one hydrogen bond acceptor group (A), mapped by the second hydroxy group and 5) other hydrophobic feature (H1) occupied by a piperidine ring.

We decided to perform docking studies to have more information about the binding mode of the prototype Ro 25-6981 (**2**) and to explore the binding site on NR2B of new potential ligands. Malherbe et al. identified critical residues that are involved in the Ro 25-6981 binding site of the NR2B subunit.[7] The data suggested that D101A and F176A mutations resulted in the complete loss of binding affinity and abolished the inhibition of NMDA-evoked currents.[7] Furthermore, mutagenesis of T233 to alanine markedly decreased the affinity of Ro 25-

6981 for the receptor by 13-fold. The mutations F182A, D104A and K234A all had a moderate influence on the binding affinity. The same authors also proposed a 3D homology model of NR2B LIVB-like domain, and we used this structure to perform a flexible docking by using GOLD. We preferred to use this methodology because the reported binding pocket was in the apo state, and we supposed that its shape could be not completely adapted to accept a ligand. Ro 25-6981 (**2**) was the molecule that was used for docking studies. The docking analysis was carried out by using the GoldScore fitness function by imposing the formation of an electrostatic interaction between the protonated nitrogen atom of the ligand and the oxygen atom of carboxylic group of the residue D101. In fact, this interaction was proposed to be the key to the anchoring of the binding pocket. The obtained complex was optimized by minimizations (10000 steps). Then the final adapted protein that was retrieved from the flexible approach was successively employed to perform a rigid docking procedure without constraints.

The best docked conformation of Ro 25-6981 is shown in Figure 3, whereas Figure 4 describes its contacts, which were calculated by LIGPLOT. As shown in Figures 3 and 4, the protonated nitrogen atom of Ro 25-6981 (**2**) is engaged in an electrostatic interaction with the carboxyl group of D101, and the phenolic OH displays a hydrogen-bonding interaction with D104; hydrophobic frames of ligands interact with hydrophobic ones that are modeled by residues T233, V42, L261, T103, A263, P278, H127, A298, I297, and F176. These findings are supported by the mutagenesis data for the ifenprodil binding site, which highlighted the crucial role of residues D101, D104, F176 and T233 for the interactions of ifenprodil-like ligands to ATD of NR2B subunit.[7]

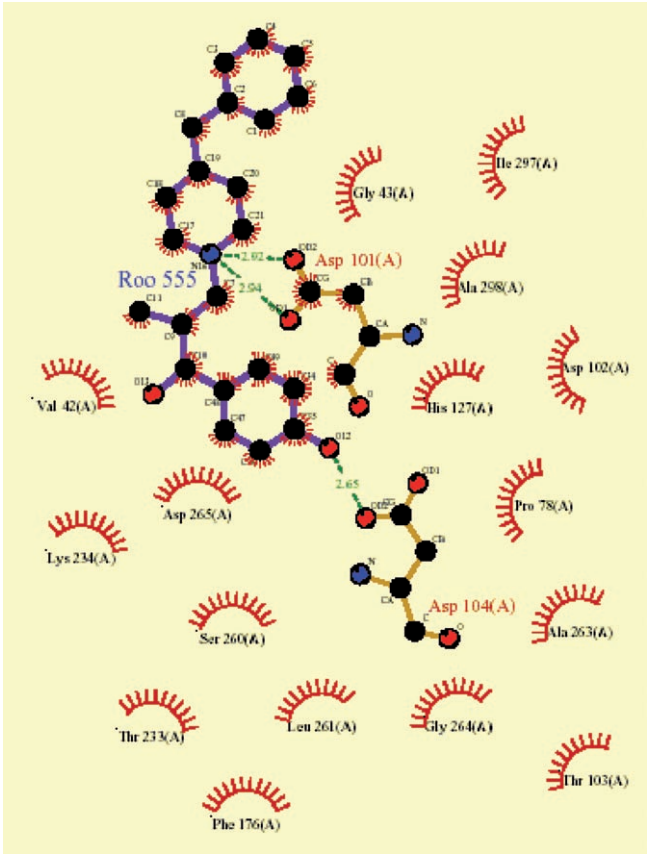

Figure 4. Contacts between Ro 25-698 (**2**) and NR2B binding pocket. Dashed lines are hydrogen bonds and 'eyelashes' show residues involved in hydrophobic interactions. Image generated with HBPLUS and LIGPLOT.

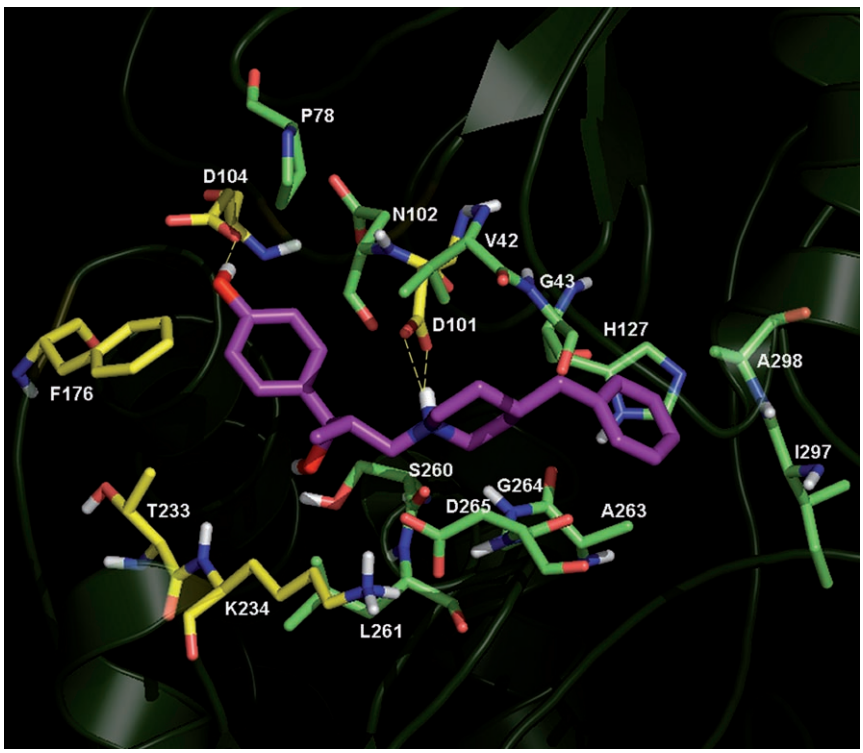

Figure 3. The best docked conformation of Ro 25-6981 (**2**) into the modeled binding pocket.

Notably, the performed structure-based studies were generally in agreement with our ligand-based experiments, which were carried out by employing HipHop Catalyst module. In fact, the 3D pharmacophore model (Figure 2) was characterized by six chemical features that were complementary to specific residues of the binding pocket constructed through docking studies. In particular, a) the positive ionizable feature (P) corresponds to negative charged region (D101); b) the hydrophobic aromatic feature (Z) of ligand interacts with F176; c) the hydrogen bond donor (D) creates contact with the acceptor fragment of D104; d) the hydrophobic fea-

tures (H1,H2) occupy the hydrophobic regions composed by following residues A298, I297, A263; whereas the hydrogen bond acceptor (A) could interact with the L234. Based on these encouraging findings and in an attempt to discover new potential NR2B ligands, we decided to use the highest rank hypothesis that was obtained as a query for database searching.

At first the six-point pharmacophore hypothesis was used to validate the obtained model by searching known NR2B ligands in the Derwent World Drug Index (WDI), a database of marketed and developmental drugs.[16] The "fast flexible search" option in Catalyst was selected. As expected, the database search retrieved compounds that had been part of our training set (**1**–**4**), but, as we hoped, other known NR2B antagonists, such as EMD-95885, 2309-BT and CP-112116, were also found.

The apparent reliability of our pharmacophore model for NR2B ligands prompted us to use it to screen the Chemicals Available for Purchase (CAP) database from Accelrys to discover new candidates. The search returned about 5000 compounds, which contained the specified 3D location of chemical functions. A subset of ~2000 structures was created by filtering compounds by their Catalyst fitness score and by considering only those with a value that was equal to or greater than 3.00. The resulting molecules were exported in a SD format file to process them by ACD/Labs software. Calculations of molecular properties were carried out by using ACD/PhysChem History, and then by using ACD/Chem Folder we selected ~400 molecules according the Lipinski rules,[17] which describe the properties of drug-like compounds.

Compounds that satisfy the reported selection criteria were retrieved and overlaid with the 3D-pharmacophore by using the "Best Fit" option and three compounds (**7**–**9**, Figure 5)

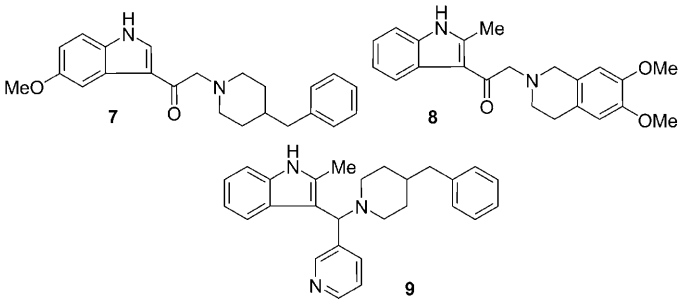

Figure 5. Hits selected as potential NR2B antagonists.

were selected for biological testing on the basis of their fit value, cost and availability. The selected compounds (**7**–**9**), which all bear an indole scaffold, were screened for their affinity for the NR2B receptor by using [^{3}H]ifenprodil as radioligand (Custom Screen by MDS Pharma Services, Taiwan) according to a published protocol.[18] Among the compounds that were tested, only the derivative 2-(4-benzylpiperidin-1-yl)-1-(5-methoxy-1*H*-indol-3-yl)ethan-1-one (**7**) showed significant binding affinity and displayed an 86% radioligand inhibition at a concentration of 10 μM. This result suggested that our 3D pharmacophore model could be useful to identify other potential NR2B ligands.

Figure 6 shows that the compound **7** fits into the 3D hypothesis in two different alignments that differ very little in their corresponding fit values (4.7 and 4.5, respectively). In Figure 6a the nitrogen atom of the piperidine nucleus occupies

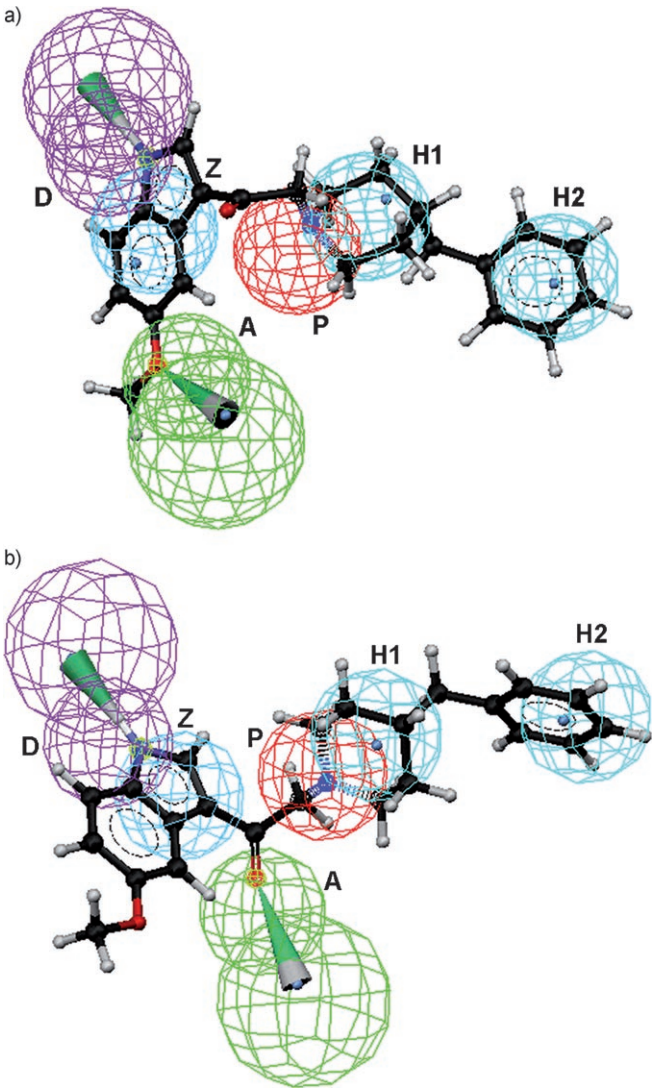

Figure 6. Mapping of the two different alignments of compound **7** onto the Catalyst pharmacophore model. Pharmacophoric features are: one positive ionizable (P, red), one hydrophobic aromatic (Z, light blue), two hydrophobic (H, cyan), one hydrogen bond donor (D, magenta), and one hydrogen bond acceptor (A, green).

the positive ionizable sphere, the indole system maps the hydrophobic aromatic area, the NH moiety of the indole is located on the hydrogen bond donor region, the methoxy substituent corresponds to the hydrogen bond acceptor region, and finally the two hydrophobic regions are occupied by the piperidine and benzyl rings. Figure 6b describes the role of the oxygen atom of carbonyl group as hydrogen bond acceptor function (A) instead the oxygen of methoxy substituent, whereas the other interactions were very similar to those found in the alignment displayed in Figure 6a.

On the basis of these results, we planned the synthesis of some analogues of compound **7** by maintaining the main skeleton; our goal was to explore the influence of the substituents on benzene fused ring. In particular, we chose to 1) remove the methoxy substituent to evaluate whether this functional group is important for recognition by the binding pocket (see Figure 6b), 2) introduce halogen atoms to consider the steric and electronic effects on benzene-fused ring, and 3) explore the steric hindrance limitation in hydrophobic area through the introduction of a benzyloxy group. These structural modifications are also focused to provide further information about the binding mode that is suggested by docking experiments such as the hydrogen bond, π-stacking, and hydrophobic interactions with the crucial residues D104, F176, and T233.

Table 1. Anticonvulsant activity of **2** and indoles **7** and **20**–**23** against audiogenic seizures in DBA/2 mice.

Compound	ED_{50} [$\mu mol\,kg^{-1}$][a]	
	clonus	tonus
Ro 25-6981 (**2**)	40.0 (21.1–54.7)	10.6 (5.16–21.8)
7	59.9 (38.7–92.7)	36.5 (26.1–51.0)
20	22.4 (13.9–36.2)	8.71 (5.71–13.3)
21	90.2 (56.8–143)	36.1 (24.5–53.4)
22	84.9 (64.7–111)	49.7 (34.8–71.0)
23	72.7 (50.8–104)	45.3 (32.2–63.6)

[a] All data were calculated according to the method of Litchfield and Wilcoxon.[29] At least 32 animals were used to calculate each ED_{50} value. The 95% confidence limits are given in parentheses.

Chemistry

As outlined in Scheme 1 the treatment of suitable indole derivatives **10**–**14** with chloroacetyl chloride gave the 3-chloroacetylindoles **15**–**19**. The intermediates **15**–**19** were then converted into 2-(4-benzylpiperidin-1-yl)-1-(1*H*-indol-3-yl)ethan-1-one derivatives **7** and **20**–**23** by reaction with benzylpiperidine in alkaline medium.

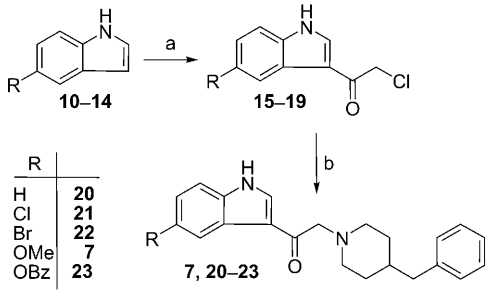

Scheme 1. Reagents and conditions: a) $ClCH_2COCl$, pyridine, dioxane, 60 °C, 2 h; b) benzylpiperidine, K_2CO_3, toluene, reflux, 3 h.

Pharmacology

In vivo activity of the synthesized 2-(4-benzylpiperidin-1-yl)-1-(1*H*-indol-3-yl)ethan-1-one derivatives (**7**, **20**–**23**) was evaluated against audiogenic seizures in DBA/2 mice. This is considered to be an excellent animal model for generalized epilepsy and for screening new anticonvulsant drugs.[19] The results were compared with the activity of Ro 25-6981 (**2**). The pharmacological results presented in Table 1 show that derivative **7** displayed modest efficacy in vivo; notably, the 2-(4-benzylpiperidin-1-yl)-1-(1*H*-indol-3-yl)ethan-1-one (**20**) was two-fold more potent than Ro 25-6981 (**2**), whereas the other synthesized compounds demonstrated less anticonvulsant potency. These results suggested that for this class of compounds the presence of a substituent on the benzene-fused ring of the indole frame negatively influenced the in vivo activity.

To ascertain its ability to interact with NR2B/NMDA receptor site, we evaluated the binding affinity for derivative **20**, which is the most active molecule of the series. This compound displayed 89% radioligand inhibition at 10 μM and an IC_{50} value of 0.769 μM. Binding affinity studies also showed that the binding on different NMDA receptor sites (agonist, glycine, phencyclidine), as well as against other ionotropic (AMPA, KA) or metabotropic glutamate receptor subtypes, was not significant at 10 μM concentration.

With the aim to define the mechanism of action of the most active compound **20**, a patch clamp study has also been performed on brain slices from the rat hippocampus, which was prepared as described previously.[20] Membrane current was recorded from single CA1 pyramidal neurons at a holding potential of −60 mV. The application of NMDA induced an inward current with a mean amplitude of 320 ± 37 pA (mean ± SEM, $n = 4$); when compound **20** was simultaneously applied, the amplitude of NMDA-mediated current was decreased (Figure 7a). The amount of decrease in the NMDA-mediated current amplitude by compound **20** ranged between 39 and 42% in different neurons, and was statistically significant in all the cases examined (Figure 7b); this indicates that this compound behaves as an antagonist of NMDA receptors. When the effect of **20** was examined as a function of time (Figure 7c), we observed that in two of the neurons the inhibition was followed by an increase of NMDA-mediated current amplitude; the mechanism for the latter effect remains to be identified.

The neuroprotective effects of the most active indoles (**7** and **20**) have been evaluated in human cortical neuronal cell line HCN-1A. We observed that these compounds protected against glutamate-induced neurotoxicity; the neuroprotective effect was assessed by measuring both neuronal viability and lactate dehydrogenase (LDH) release. In particular, we observed that the exposure of differentiated HCN-1A cells cultures to glutamate (100 μM) for 24 h induced a significantly higher LDH release than control (55 ± 4%) and a significant decrease of neuronal MTT levels (47 ± 8% reduction relative to control); whereas the pre-exposure to indole derivatives (**7** and **20**) at different doses (see Experimental Section) significantly prevented the LDH release (25–50% decrease relative to glutamate-treated cells) and decreased the glutamate-induced MTT levels (30–40% reduction relative to glutamate-treated cells).

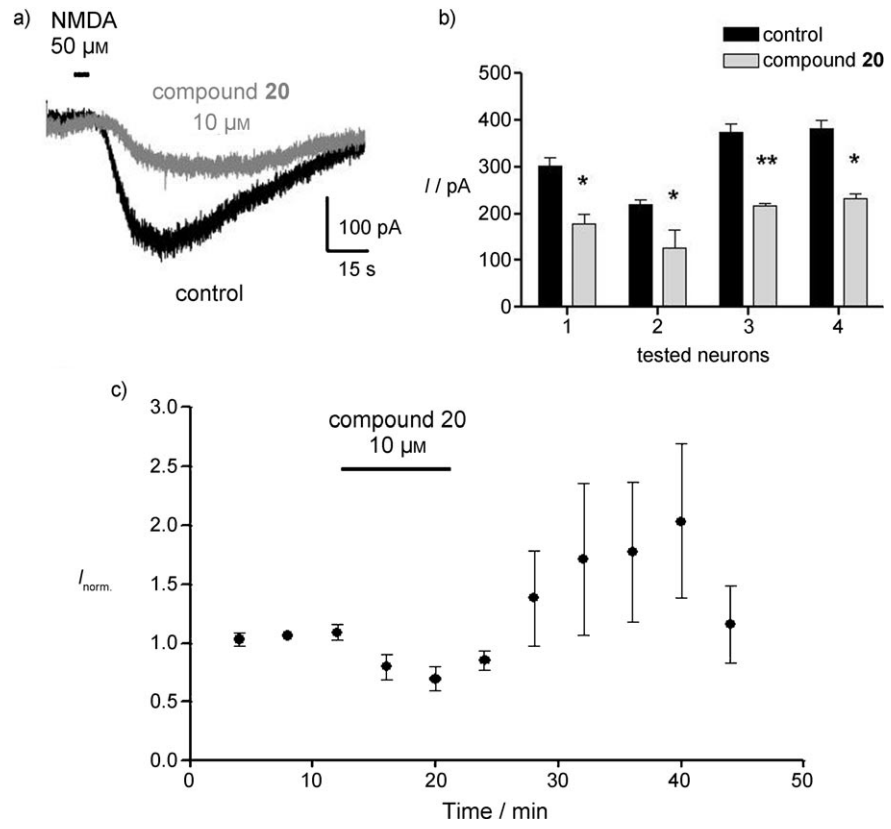

Figure 7. Effects of compound **20** on NMDA receptor-mediated current. a) Application of NMDA (50 μM, 5 s) induced in CA1 pyramidal neurons an inward current, the amplitude of which was decreased during application of compound **20** (10 μM, 5 min). b) In the presence of compound **20**, the amplitude of NMDA-mediated current (gray columns) was significantly smaller (*$p < 0.01$, **$p < 0.001$, t-test) than in control conditions (black columns). c) NMDA-mediated current amplitude values (normalized with respect to control) from all the tested neurons (mean ± SEM, $n = 4$) were pooled and are represented as a function of time; this shows that inhibition of NMDA-mediated current by compound **20** was reversible. In two cases, inhibition of NMDA-mediated current was followed by an increase.

Upon microscopic inspection, control cultures exhibited morphological indicators of viability; neurons (multipolar or bipolar) with numerous long and extensively branched processes with spines and varicosities were observed. Glutamate-treated cultures showed severe morphological damage (cell condensation, vacuole formation, retracted dendrites and round, shrunken cell bodies), whereas after the pre-treatment with 1 μM of compounds **7** and **20** the cells were relatively undamaged by 100 μM of glutamate (Figure 8). Furthermore none of the molecules that we examined were toxic to the cultures in the absence of glutamate, and the molecules alone had no effect on cell viability compared with untreated cells as measured by the MTT or trypan blue test (data not shown).

Docking studies

With the aim to deepen our study, we docked the most active indole derivative **20** in the proposed binding pocket that was modeled by computational methodologies (Figure 9). In particular, in our structure-based studies (see molecular modeling studies section) we described the binding pocket of the ifenprodil-like recognition site and the main contacts of the selective ligand Ro 25-6981 (**2**) with the crucial amino acid residues by taking into account the previously reported mutagenesis data.[7] Figure 9 shows the best docking results of 2-(4-benzylpiperidin-1-yl)-1-(1*H*-indol-3-yl)ethan-1-one (**20**) into the proposed binding pocket and its main interactions. This pose was selected on the basis of the GOLD fitness score; the bound conformation with the highest fitness score was chosen as the predicted ligand binding mode.

The comparison of Figure 3 and 9 highlights that Ro 25-6981 (**2**) and **20** share a similar binding mode to the NR2B ifenprodil-like pocket, in spite of some different interactions. Analogously to Ro 25-6981 (**2**), the protonated nitrogen atom of compound **20** is involved in an electrostatic interaction with the carboxyl group of D101; this confirms the important role that it plays in ligand binding. Interestingly, the aromatic ring of the indole system and benzylpiperidine fragment of compound **20** interacted with specific areas to establish several favorable hydrophobic interactions. Moreover, compound **20** displayed a H-bonding interaction between the NH of the indole ring and E235 (Figure 7).

Conclusions

Recent studies had shown that allosteric modulators of NR2B/NMDA are able to bind with a specific region located into NTD of the NR2B subunit and site-directed mutagenesis data had described the key residues for binding pocket. In this study we have used a combination of ligand-based and structure-based methodologies; this led to the identification and validation of new potential ligands that contain the indole nucleus. Their synthetic pathway was performed and the new compounds that were obtained were tested in vivo as anticonvulsant agents. With the aim to understand the mechanism of action, we tested their affinity to NR2B ifenprodil-like recognition site and evaluated their ability to decrease NMDA receptor-mediated current in patch clamp experiments. Moreover, we studied the neuroprotective effects of the most active indole derivatives in HCN-1A human cortical neuronal cells. The results that were obtained suggest that the compound **20** could be con-

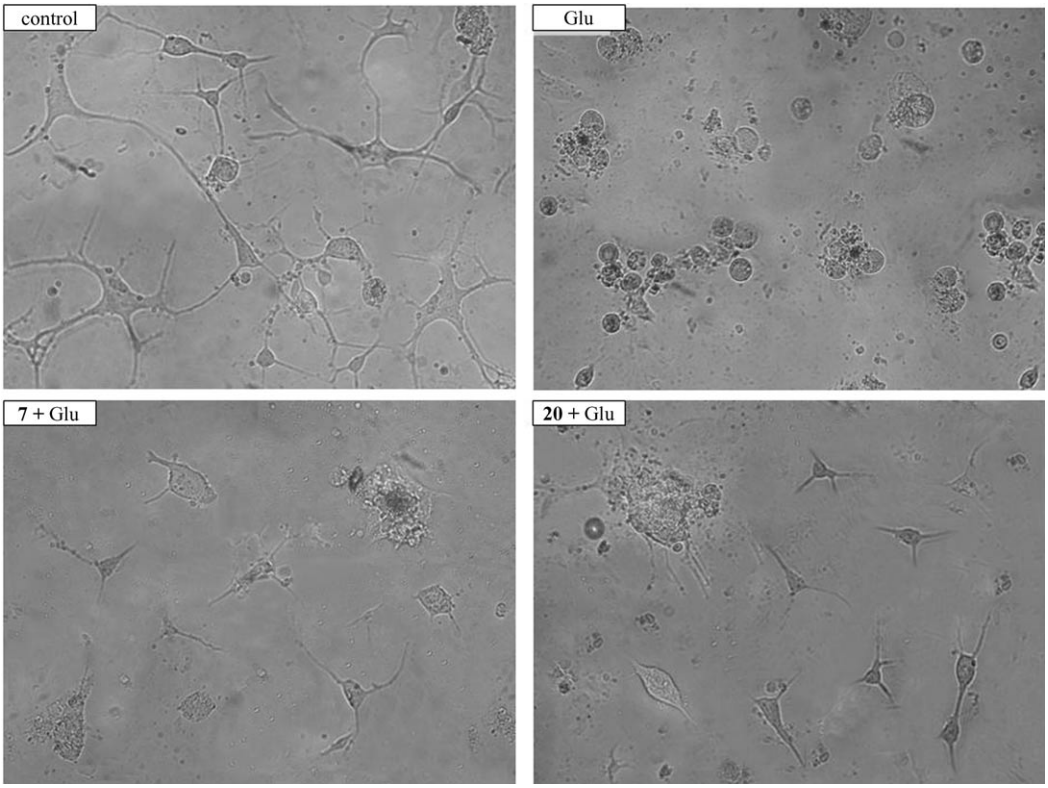

Figure 8. Changes in cell morphology after pretreatment with compounds **7** and **20** (1 μM) on glutamate (100 μM)-induced neurotoxicity in HCN-1A neurons.

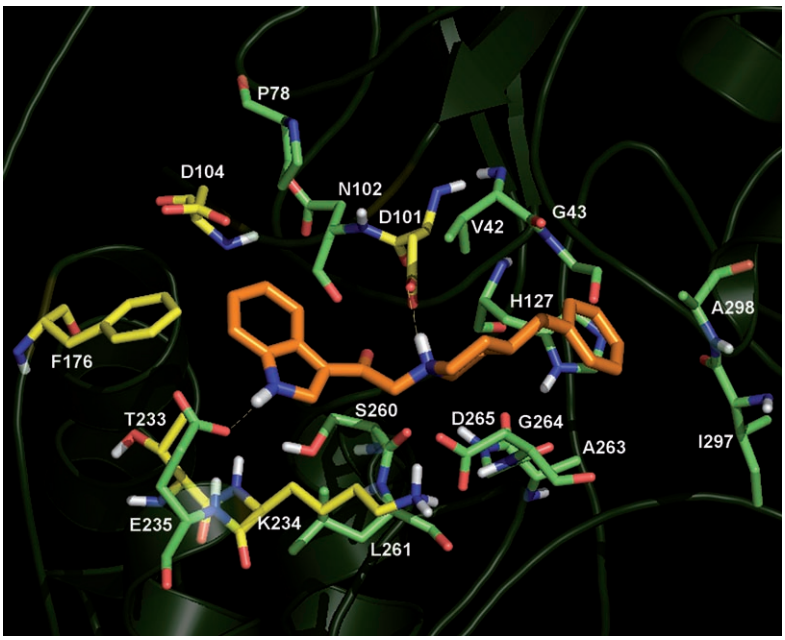

Figure 9. The binding mode of compound **20** in the modeled binding pocket.

sidered to be a new interesting neuroprotective agent and could provide a starting point to develop new NR2B antagonists.

Experimental Section

Computational methods

Pharmacophore modeling: For pharmacophore model generation we used the HipHop algorithm that was implemented in the Catalyst software package version 4.10 (Catalyst version 4.10, Accelrys), which was run on a SGI O2+ R12000 workstation. HipHop compares diverse molecules to derive 3D hypotheses that are based on common chemical features, without considering activity.[21] Derivatives **1**–**6** were selected as a training set (TS), and all structures were generated by using the 2D/3D editor sketcher in Catalyst and submitted to energy minimization and conformational analysis (max. number of conformers = 250, generation type: best quality, energy range = 10 kcal mol−1). The absolute stereochemistry of the asymmetric carbon atoms in compounds **2**, **3**, and **5**, which provided the optimal biological activity has been reported in the literature and was therefore assigned accordingly. In the case of ifenprodil (**1**), little or no difference in affinity for the NR2B receptor has been found for the (±)-erythro and (±)-threo-ifenprodil race-

mates,[22] and it was therefore left to the Catalyst program to assign the optimal stereochemistry for this compound. Usually in such cases Catalyst fixes the stereochemistry as "unknown". Catalyst provided a dictionary of chemical features that have been found to be important in ligand–target interactions. These are hydrogen bond donors, hydrogen bond acceptors, aromatic rings, hydrophobic (aliphatic or aromatic) groups, and positive and negative ionizable groups. The pharmacophore features that were considered in this study were hydrogen bond donor (D), hydrogen bond acceptor (A), hydrophobic groups (H), hydrophobic aromatic region (Z) and positive ionizable (P). The interfeature spacing penalty was decreased from its default value to 50 pm. No constraint on the minimum and maximum number of each type of feature in the reported pharmacophores was applied. In the model generation methodology, the highest weighting was given to Ro 25-6981, which represents the reference compound for this class of ligands.[23]

Database searching: The pharmacophore model that was built within the Catalyst software was used for 3D-database searching on Derwent World Drug Index (WDI), which contains drugs and other bioactive molecules, and on Chemicals Available for Purchase (CAP), which is a collection of compounds from chemical suppliers. In Catalyst, two algorithms for database searching could be chosen: the Fast Flexible Search and the Best Flexible Search. The first one can be considered to be a semirigid search technique (it uses the full conformational model of a molecule stored in the database, but does not modify the geometry of the pre-computed conformations); the second one was a real flexible search tool (it uses the conformational model stored in the database and it is allowed to flex the molecules to map to the query).[24] In our study, all screening experiments were performed by using the Fast Flexible Search algorithm.

Automated molecular docking experiments: Prior to docking, the ligand structures were built by using standard bond lengths and angles from the Sybyl 8.2 fragment library and fully optimized by the semiempirical quantum mechanical method AM1. Ligands were modeled in their nitrogen-protonated form. The crystal structure of NR2B was sent by Dr. P. Malherbe (see Acknowledgements). Automated docking studies were then performed by using CCDC's GOLD (Genetic Optimization for Ligand Docking) software version 3.1.1.[25] GOLD allowed for partial protein flexibility, and the following residues lining the binding pocket were given full flexibility to move during docking: V42, T76, D77, K79, D101, D104, P176, T233, K234. An active site of 10.0 Å radius was defined, which was centered on the α-carbon atom of residue D101. A hydrogen bond constraint was set: the hydrogen of the protonated nitrogen of Ro 25-6981, and of the ligands and the carboxylate oxygen atom of the residue D101. The best docking complex was then energy-minimized by using the CHARMM v22 force field.[26] The whole system was minimized for 1000 steps of steepest-descent minimization until RMS = 0.5 and 1000 steps of conjugated gradients algorithm until RMS = 0.5. Finally this structure was used to perform a new docking procedure without protein flexibility and constraints. An active site of 10.0 Å radius was defined, which was centered on the position of ligand Ro 25-6981. For all calculations the GOLD score was chosen as a fitness function, and the standard default settings were used in all the calculations. For each of the 100 independent genetic algorithm runs, a default maximum of 100000 genetic operations was performed by using the default operator weights and a population size of 100 chromosomes. Default cutoff values of 2.5 Å for hydrogen bonds and 4.0 Å for van der Waals interactions were employed. Results that differed by less than 1.5 Å in ligand–all-atom RMSD were clustered together.

Chemistry

All commercially available reagents were obtained from Aldrich and used without further purification. Melting points were determined on a Stuart SMP10 apparatus and are uncorrected. Elemental analyses (C, H, N) were carried out on a Carlo Erba Model 1106 Elemental Analyzer and the results are within $\pm 0.4\%$ of the theoretical values. Merck silica gel 60 F254 plates were used for analytical TLC. Flash chromatography was carried out on a Biotage SP4 EXP. ^{1}H NMR spectra were measured in $CDCl_3$ with a Varian Gemini 300 spectrometer; chemical shifts are expressed in δ (ppm) relative to TMS as internal standard and coupling constants (*J*) in Hz. All exchangeable protons were confirmed by the addition of D_2O.

General procedure for the synthesis of 2-(4-benzylpiperidin-1-yl)-1-(1*H*-indol-3-yl)ethan-1-one derivatives (7, 20–23): A solution of chloroacetyl chloride (169 mg, 0.0015 mol) in dioxane (0.25 mL) was added dropwise to a solution of indole derivative (10–14) (0.001 mol) and pyridine (0.122 mL, 0.0015 mol) in dioxane (0.75 mL). The mixture was stirred for 2 h at 60 °C, then it was cooled to room temperature, poured into H_2O (20 mL) and extracted with EtOAc. The organic phase was dried over Na_2SO_4, and the solvent was removed under reduced pressure to give a crude residue. Purification by flash chromatography ($CHCl_3$/MeOH, 9:1) afforded the 3-chloroacetylindole derivatives (**15**–**19**) as white solids. Then derivatives **15**–**19** (0.001 mol), benzylpiperidine (175 mg, 0.001 mol) and K_2CO_3 (0.0005 mol) were heated at reflux in toluene (5 mL) for 3 h. The organic phase was filtered, and the solvent was removed under reduced pressure. The residue was powdered by treatment with Et_2O and recrystallized from EtOH to give desired compounds (**7**, **20**–**23**). ^{1}H NMR spectral data confirmed the structure of 3-chloroacetylindole intermediates **15**–**19** and were in accordance with literature.[27,28]

2-(4-Benzylpiperidin-1-yl)-1-(5-methoxy-1*H*-indol-3-yl)ethan-1-one (7): yield 70%; mp: 177 °C; ^{1}H NMR ($CDCl_3$): $\delta = 1.36$–3.00 (m, 9H), 2.54 (d, $J = 6.86$, 2H), 3.58 (s, 2H), 3.89 (s, 3H), 6.92 (dd, $J = 8.79$, $J = 2.47$, 1H), 7.13–7.32 (m, 5H), 7.93 (d, $J = 2.47$, 1H), 8.33 (br s, 1H), 8.47 ppm (br s, 1H, NH); elemental analysis calcd for $C_{23}H_{26}N_2O_2$: C 76.21, H 7.23, N 7.73, found: C 76.34, H 7.52, N 7.51.

2-(4-Benzylpiperidin-1-yl)-1-(1H-indol-3-yl)ethan-1-one (20): yield 25%; mp: 210 °C; ^{1}H NMR ($CDCl_3$): $\delta = 1.24$–3.01 (m, 9H), 2.55 (d, $J = 6.87$, 2H), 3.60 (s, 2H), 7.10–7.30 (m, 7H), 7.40 (m, 1H), 8.37 (br s, 1H), 8.40 (br s, 1H), 8.42 ppm (br s, 1H; NH); elemental analysis calcd for $C_{22}H_{24}N_2O$: C 79.48, H 7.28, N 8.43, found: C 79.34, H 7.52, N 8.51.

2-(4-Benzylpiperidin-1-yl)-1-(5-bromo-1*H*-indol-3-yl)ethan-1-one (21): yield 32%; mp: 230 °C ^{1}H NMR ($CDCl_3$): $\delta = 1.35$–3.00 (m, 9H), 2.54 (d, 2H, $J = 6.86$), 3.58 (s, 2H), 7.12–7.36 (m, 7H), 8.39 (br s, 1H), 8.58 (br s, 1H), 8.65 ppm (br s, 1H, NH); elemental analysis calcd for $C_{22}H_{23}BrN_2O$: C 64.24, H 5.64, N 6.81, found: C 64.34, H 5.52, N 6.51.

2-(4-Benzylpiperidin-1-yl)-1-(5-chloro-1*H*-indol-3-yl)ethan-1-one (22): yield 36%; mp: 232 °C ^{1}H NMR ($CDCl_3$): $\delta = 1.35$–3.00 (m, 9H), 2.54 (d, 2H, $J = 6.87$), 3.59 (s, 2H), 7.11–7.33 (m, 7H), 8.37 (br s, 1H), 8.40 (br s, 1H), 8.42 ppm (br s, 1H; NH); elemental analysis calcd for $C_{22}H_{23}ClN_2O$: C 72.02, H 6.32, N 7.64, found: C 72.36, H 6.42, N 7.59.

1-(5-Benzyloxy-1*H*-indol-3-yl)-2-(4-benzylpiperidin-1-yl)ethan-1-one (23): yield 80%; mp: 196 °C ^{1}H NMR ($CDCl_3$): $\delta = 1.35$–3.00 (m,

9H), 2.54 (d, $J=6.87$, 2H),3.57 (s, 2H), 5.14 (s, 2H), 6.98–7.50 (m, 12H), 8.04 (brs, 1H), 8.33 (brs, 1H), 8.49 ppm (brs, 1H, NH); elemental analysis calcd for $C_{28}H_{28}N_2O_2$: C 79.22, H 6.65, N 6.60, found: C 79.11, H 6.49, N 6.58.

Pharmacology

Testing of anticonvulsant activity: All experiments were performed with DBA/2 mice that were genetically susceptible to sound-induced seizures. The DBA/2 mice (8–12 g; 22–25-days-old) were purchased from Harlan Italy (Corezzana, Milan, Italy). Groups of 10 mice of either sex were exposed to auditory stimulation 30 min following administration of vehicle or each dose of drugs studied. The compounds were given intraperitoneally (i.p.) (0.1 mL/10 g of body weight of the mouse) as a freshly prepared solution in 30% dimethyl sulfoxide (DMSO) and 70% sterile saline (0.9% NaCl). Individual mice were placed under a hemispheric perspex dome (diameter 58 cm), and 60 s were allowed for habituation and assessment of locomotor activity. Auditory stimulation (12–16 kHz, 109 dB) was applied for 60 s or until tonic extension occurred, and induced a sequential seizure response in control DBA/2 mice; this consisted of an early wild running phase, followed by generalized myoclonus and tonic flexion and extension sometimes followed by respiratory arrest. The control and drug-treated mice were scored for latency to, and incidence of the different phases of the seizures. The experimental protocol and all the procedures that involved animals and their care were conducted in conformity with the institutional guidelines and the European Council Directive of laws and policies. Statistical comparisons between groups of control and drug-treated animals were made by using Fisher's exact probability test (incidence of the seizure phases). The ED_{50} values of each phase of audiogenic seizures was determined for each dose of compound administered, and dose–response curves were fitted by using the Litchfield and Wilcoxon method through a computer program.[29]

Receptor binding studies: The radioligand binding assays were carried out by using the specific ligands [^{3}H]AMPA, [^{3}H]CGP 39653, [^{3}H]kainic acid, [^{3}H]MDL-105519, [^{3}H]TCP, [^{3}H]L-glutamic acid and [^{3}H]ifenprodil (Custom Screen by MDS Pharma Services, Taiwan).[30]

Electrophysiology: Young Wistar rats (age 9–17 days) were decapitated under diethyl ether anesthesia, their brains were rapidly removed, placed in oxygenated ice-cold artificial cerebrospinal fluid (ACSF; composition in mM: NaCl 124, KCl 3.0, NaH_2PO_4 1.2, $MgSO_4$ 1.2, $CaCl_2$ 2.0, $NaHCO_3$ 26, D-glucose 10, pH 7.3) and cut into 300-μm slices with a vibratome. One slice that contained the hippocampus was then transferred to the recording chamber of a patch clamp set-up, continually perfused with oxygenated ACSF and viewed under an IR differential interference contrast microscope (Leica DMLFS). CA1 pyramidal neurons were visually identified by their location and by their typical shape and dimension. Membrane current was recorded from single CA1 pyramidal neurons with the patch clamp technique in the whole-cell configuration by using an L/M-EPC7 amplifier (List Electronic, Germany). The recording electrode was a glass micropipette (resistance 1.5–3 MΩ) that was filled with intracellular solution (composition in mM: K-gluconate 170, HEPES 10, NaCl 10, $MgCl_2$ 2, EGTA 0.2, Mg-ATP 3.5, Na-GTP 1, pH 7.3). Capacitive currents were electronically cancelled and series resistance was compensated by 60–80%. Data were acquired and analyzed by using EPC and Signal software (Cambridge Electronic Design, England). Immediately after the beginning of recording, the slice was perfused with a Mg^{2+}-free ACSF that contained tetrodotoxin (TTX, 1 μM, Tocris) to prevent synaptic activity. *N*-methyl-D-aspartic acid (NMDA, 50 μM, Sigma) was dissolved in Mg^{2+}-free ACSF that contained glycine (0.5 μM, Sigma) and was applied during 5 s by using a computer-controlled electrovalve solution changer (MSC-200, Bio-Logic, Claix, France). Compound **20** was dissolved in Mg^{2+}-free ACSF and applied by bath perfusion at a flow rate of 1 mL min^{-1}. The holding potential of CA1 pyramidal neurons was set at −60 mV and membrane current was continually recorded at an acquisition rate of 4 KHz. Several pulses of NMDA were applied for each neuron respectively in control conditions and during application of 20 (10 μM, 5 min) through the bath perfusion system. NMDA-induced current amplitude was measured as the difference between peak current amplitude and baseline. For each neuron that was studied, the amplitude of at least three consecutive NMDA-induced currents were measured respectively in control conditions and in the presence of compound **20** and the two sets of raw values were compared by using Student's unpaired t-test (Graph Pad software, La Jolla, CA, USA). To illustrate the time course of effects, NMDA-mediated current amplitude was normalized by dividing by the mean amplitude value calculated from at least three NMDA responses in control conditions. Normalized NMDA-mediated currents from all the responsive neurons were pooled (mean ± SEM) and represented on a graphic as a function of time.

Neuroprotective efficacy in human cortical cell line HCN-1A: The HCN-1A cell line (Catalog number CRL-10442), media (Catalog number 30-2002) and fetal bovine serum for cell culture were obtained from the American Type Culture Collection (ATCC, Manassas, VA, USA). The HCN-1A cells were derived from cortical tissue that was removed from a patient who was undergoing hemispherectomy for intractable seizures. Chemicals and biochemicals were obtained from Sigma–Aldrich (Milan, Italy) and from Cambrex Bio Science S.r.l. (Milan, Italy) or LGC Promochem S.r.l. (Sesto San Giovanni, Milan, Italy). HCN-1A cells were cultured in Dulbecco's modified Eagle's medium that contained 10% fetal bovine serum (pH 7.35) and antimycotic (1% *v/v*). The cells were maintained at 37 °C in 5% CO_2. For differentiation experiments, cells were cultured in 96-well plates at 5000 cells per well. Differentiation of these neuronal cells was induced by adding fresh medium that contained 25 ng mL^{-1} β-nerve growth factor (β-NGF), 0.5 mM dibutyryl cyclic AMP (dbcAMP) and 0.5 mM 3-isobutyl-1-methylxanthine (IBMX). When the neurons became differentiated and developed neuritic processes, various concentration of compound **7** (1.3×10^{-4}, 1.3×10^{-3}, 1.3×10^{-2} mM), or compound **20** (1.5×10^{-4}, 1.5×10^{-3}, 1.5×10^{-2} mM) and glutamate (0.01, 0.1, 1, and 5 mM) were added in a total volume of 100 μL. After 24 h, cell viability was determined by using the MTT cell proliferation assay and Trypan blue test. The cell viability results were verified in all experiments by using the lactate dehydrogenase cytotoxicity assay (LDH). For cell viability the MTT (3-(4,5-dimethylthiazol-2-yl-)-2,5-diphenyltetrazolium bromide)[31] or the trypan blue dye exclusion method[32] were used. Morphology, differentiation and density of cells were determined microscopically with an inverted microscope that was equipped with phase-contrast optics (Optika Microscopes). Cells were incubated for 24 h with glutamate and/or compounds **7** and **20**. After this period a MTT solution (10 μL of a 5 mg mL^{-1} solution in PBS) was added and incubated for 3 h. MTT is reductively converted into a blue formazan derivative, which is quantified photometrically at 570 nm by using an ELISA microplate reader (Bio Rad 550, Bio-Rad Laboratories). The measurement of cellular MTT reduction was assessed in quadruplicate, and the data were expressed as the mean ± SEM. Trypan blue selectively stained cells with damaged plasma membrane and had no access to intact cells. Cells were stained with trypan blue (0.4% in PBS with HBSS buffer, 1:1) for 10 min at 37 °C

under 5% CO_2. Viable and nonviable (blue cells) cells were counted on a hematocytometer (Marienfeld, Germany). Three independent counts of cells were made for each aliquot. LDH release into the culture media was measured by using a cytotoxicity assay kit from Sigma, and the absorption was read at 490 nm by using an ELISA reader (Bio Rad 550).[33] Statistical comparison was carried out by using one-way analysis of variance (ANOVA) and Dunnet's test. The data represent means $\pm$SEM and values of $P < 0.05$ were statistically significant.

Acknowledgements

We thank Dr. P. Malherbe for providing us more detailed results of his 3D homology model of the NR2B LIVB-like domain. Financial support for this research by the University of Messina and MiUR is gratefully acknowledged.

Keywords: anticonvulsant activity · HCN-1A neurons · molecular modeling · neurotransmitters · NR2B/NMDA antagonists

[1] M. L. Mayer, *Curr. Opin. Neurobiol.* **2005**, *15*, 282–288.
[2] J. N. Kew, J. A. Kemp, *Psychopharmacology* **2005**, *179*, 4–29.
[3] G. Kohr, *J. Physiol.* **2007**, *581*, 1–2.
[4] P. Paoletti, J. Neyton, *Curr. Opin. Pharmacol.* **2007**, *7*, 39–47.
[5] P. Paoletti, F. Perin-Dureau, A. Fayyazuddin, A. Le Goff, I. Callebaut, J. Neyton, *Neuron* **2000**, *28*, 911–925.
[6] L. Marinelli, S. Cosconati, T. Steinbrecher, V. Limongelli, A. Bertamino, E. Novellino, D. A. Case, *ChemMedChem* **2007**, *2*, 1498–1510.
[7] P. Malherbe, V. Mutel, C. Broger, F. Perin-Dureau, J. A. Kemp, J. Neyton, P. Paoletti, J. N. Kew, *J. Pharmacol. Exp. Ther.* **2003**, *307*, 897–905.
[8] K. R. Gogas, *Curr. Opin. Pharmacol.* **2006**, *6*, 68–74.
[9] I. Borza, G. Domany, *Curr. Top. Med. Chem.* **2006**, *6*, 687–695.
[10] P. L. Chazot, *Curr. Med. Chem.* **2004**, *11*, 389–396.
[11] J. A. McCauley, *Expert Opin. Ther. Pat.* **2005**, *15*, 389–407.
[12] B. L. Chenard, F. S. Menniti, *Curr. Pharm. Des.* **1999**, *5*, 381–404.
[13] J. M. Loftis, A. Janowsky, *Pharmacol. Ther.* **2003**, *97*, 55–85.
[14] S. S. Nikam, L. T. Meltzer, *Curr. Pharm. Des.* **2002**, *8*, 845–855.
[15] A. P. Tamiz, E. R. Whittemore, Z. L. Zhou, J. C. Huang, J. A. Drewe, J. C. Chen, S. X. Cai, E. Weber, R. M. Woodward, J. F. Keana, *J. Med. Chem.* **1998**, *41*, 3499–3506.
[16] Derwent World Drug Index: http://scientific.thomsonreuters.com/products/wdi/ (last access June 29, 2008).
[17] C. A. Lipinski, F. Lombardo, B. W. Dominy, P. J. Feeney, *Adv. Drug Delivery Rev.* **1997**, *23*, 3–25.
[18] H. Schoemaker, J. Allen, S. Z. Langer, *Eur. J. Pharmacol.* **1990**, *176*, 249–250.
[19] G. De Sarro, A. Chimirri, A. De Sarro, R. Gitto, S. Grasso, P. Giusti, A. G. Chapman, *Eur. J. Pharmacol.* **1995**, *294*, 411–422.
[20] L. Ciranna, S. Cavallaro, *Exp. Neurol.* **2003**, *184*, 778–784.
[21] Accelrys, Catalyst: http://www.accelrys.com (last access: August 28, 2008).
[22] P. Avenet, J. Leonardon, F. Besnard, D. Graham, J. Frost, H. Depoortere, S. Z. Langer, B. Scatton, *Eur. J. Pharmacol.* **1996**, *296*, 209–213.
[23] G. Fischer, V. Mutel, G. Trube, P. Malherbe, J. N. C. Kew, E. Mohacsi, M. P. Heitz, J. A. Kemp, *J. Pharmacol. Exp. Ther.* **1997**, *283*, 1285–1292.
[24] Accelrys Inc., San Diego, CA (USA) **2006**: http://www.accelrys.com/reference/cases/studies/catalystdb_full.html (last access June 29, 2008).
[25] G. Jones, P. Willett, R. C. Glen, A. R. Leach, R. Taylor, *J. Mol. Biol.* **1997**, *267*, 727–748.
[26] B. R. Brooks, R. E. Bruccoleri, B. D. Olafson, D. J. States, S. Swaminathan, M. Karplus, *J. Comput. Chem.* **1983**, *4*, 187–217.
[27] W. P. Deng, G. Nam, J. F. Fan, K. L. Kirk, *J. Org. Chem.* **2003**, *68*, 2798–2802.
[28] V. Hasimbegovic, J. Slatt, J. Bergman, T. Janosik, *J. Heterocycl. Chem.* **2007**, *44*, 1213–1217.
[29] J. T. Litchfield, Jr., *J. Pharmacol. Exp. Ther.* **1949**, *97*, 399–408, 393.
[30] MDS Pharma Services, Taiwan: http://www.mdsps.com/ (last access June 29, 2008).
[31] D. M. Morgan, *Methods Mol. Biol.* **1998**, *79*, 179–183.
[32] L. Black, M. C. Berenbaum, *Exp. Cell Res.* **1964**, *35*, 9–13.
[33] D. Lobner, *J. Neurosci. Methods* **2000**, *96*, 147–152.

Received: April 21, 2008
Revised: June 26, 2008
Published online on September 2, 2008

